THE ASTROPHYSICAL JOURNAL, 532:214–220, 2000 March 20

ON THE ORIGIN OF THE TULLY-FISHER RELATION

JIN KODA AND YOSHIAKI SOFUE
Institute of Astronomy, University of Tokyo, Mitaka, Tokyo 181-8588, Japan
AND
KEIICHI WADA
National Astronomical Observatory, Mitaka, Tokyo 181-8588, Japan
Received 1999 October 29; accepted 1999 November 1

ABSTRACT

We discuss the origin of the Tully-Fisher (TF) relation using the N-body/smoothed particle hydrodynamics method, which includes cooling, star formation, and stellar feedback of energy, mass, and metals. We consider initially rotating overdense spheres and trace formation processes of disk galaxies from $z = 25$ to $z = 0$ in the cold dark matter cosmology. To clarify the origin of the TF relation, we simulate formation of 14 isolated galaxies with different masses and spin parameters and compute observable values, such as the total magnitude and the line width. We find that the simulated galaxies reproduce the slope and scatter of the TF relation: the slope is originated in the difference of total galactic masses, and the scatter is produced by the difference of initial spin parameters. As well as the TF relation, observed features of spiral galaxies, such as the exponential light profile and the flat rotation curve, are reproduced in our simulations, which were assumed a priori in past semianalytical approaches.

Subject headings: galaxies: evolution — galaxies: formation — galaxies: kinematics and dynamics — galaxies: statistical

1. INTRODUCTION

The Tully-Fisher relation (Tully & Fisher 1977; hereafter TF) is one of the most basic relations in spiral galaxies and would be a clue to understanding the origin of disk galaxies. The TF relation has been roughly considered as a product of the virial theorem and a nearly constant mass-to-light ratio since its discovery. Recently, the origin of the TF relation is discussed by, e.g., Silk (1997) and Mo, Mao, & White (1998).

In their semianalytical approach, Mo et al. (1998) succeeded in reproducing the TF relation, assuming a constant mass-to-light ratio and empirical profiles of disks and halos. Heavens & Jimenez (1999) took the same approach, but included an empirical star formation model and reproduced the TF relation in four passbands simultaneously. In these semianalytical approaches, however, observed features of galaxies, such as the exponential profile and flat rotation curve, were not constructed as the results of simulations, but assumed a priori. Steinmetz & Navarro (1999) performed direct simulations of galaxy formation within the cosmological context and also succeeded in getting the slope and scatter of the TF relation. They treated the volume much larger than the scale of galaxies, and considered environmental effects (e.g., tidal field and infall/outflow of mass). However, due to the complicated behaviors of these effects, it still remains unknown what physics produces the TF relation.

Based on these arguments, we simulate formation and evolution of galaxies with the N-body/smoothed particle hydrodynamics (SPH) method including cooling, star formation, and their feedback of energy, mass, and metals to the interstellar medium (ISM). Using a similar method, Katz (1992) and Steinmetz & Müller (1994, 1995) succeeded in constructing internal structures as observed in spiral galaxies, e.g., the exponential density profile, flat rotation curve, and distributions of stellar age and metallicity in the bulge, disk, and halo. In contrast to their simulations of single galaxy formation, we consider formation of many galaxies with different masses and spin parameters. In order to investigate what physics produces the TF relation, we concentrate on formation of isolated galaxies with different initial conditions. We note that as well as the TF relation, observed features of spiral galaxies, such as the exponential light profiles and flat rotation curve, are reproduced in our simulations, which were assumed a priori in past semianalytical approaches.

2. METHODS

2.1. *Numerical Methods*

We use a GRAPE-SPH code, a hybrid scheme of the SPH and the N-body integration hardware GRAPE-3 (Sugimoto et al. 1990), the code that was first discussed by Steinmetz (1996) and developed further by us (Koda, Wada, & Sofue 2000). The code is implemented to treat three-component systems—the gas, stars, and dark matter—and calculate gravitational and hydrodynamical forces, which are symmetrized to satisfy Newton's third law. We consider the radiative and inverse Compton cooling of the gas which is optically thin and in collisional ionization equilibrium of H and He ($X_{\rm H} = 0.76$, $X_{\rm He} = 0.24$; see Katz et al. 1996). We also take phenomenological models of star formation and their feedback to mimic real galaxy formation.

The star formation model adopted is basically the same as those discussed in Katz (1992), Navarro & White (1993), and Steinmetz & Müller (1994, 1995). Stars are formed in regions that are locally contracting and Jeans-unstable at a rate given by $\dot{\rho}_* = c_* \rho_{\rm gas}/\max(\tau_{\rm dyn}, \tau_{\rm cool})$. Here, ρ_*, $\rho_{\rm gas}$, $\tau_{\rm dyn}$, and $\tau_{\rm cool}$ are the densities of stars and the gas, local dynamical, and cooling timescales, respectively. In most cases, $\tau_{\rm dyn}$ is larger than $\tau_{\rm cool}$, and the star formation timescale is typically $\sim 20\tau_{\rm dyn}$ under the adopted parameter $c_* = 0.05$. When one-third of the mass in a gas particle is transformed into stars, we create a new collisionless *star*

particle, which inherits the position and velocity of its parent gas particle.

We take a simple model of feedback. Massive stars with $\geq 8\ M_\odot$ are assumed to release energy, mass, and metals into the surrounding gas at a constant rate through stellar wind (SW) and Type II supernovae (SNe II). All of the massive stars then become white dwarfs, and 15% of them result in Type Ia supernovae (SNe Ia; Tsujimoto et al. 1995). In Table 1, we list total released energy, mass, and metal per star and the periods of feedback (see Nomoto et al. 1997a, 1997b; Yoshii, Tsujimoto, & Nomoto 1996). We can estimate the number of stars with $\geq 8\ M_\odot$, in a *star particle*, with the initial mass function (IMF) of Salpeter (1955). Released energy is provided into the surrounding gas as thermal energy. Since stars are formed and release energy at dense gas regions where feedback energy is soon radiated away, feedback does not much affect the simulations in our model.

2.2. *Initial Conditions*

We simulate formation and evolution of galaxies from $z = 25$ to 0 in the CDM cosmology ($\Omega_0 = 1$, $H_0 = 100h = 50$ km sr^{-1} Mpc^{-1}). Our initial conditions are similar to those of Katz (1992) and Steinmetz & Müller (1994, 1995), but we consider 14 isolated spheres, on which small-scale CDM fluctuations are superimposed with the Zeldovich approximation (Zeldovich 1970). The densities of the spheres are enhanced above the background field by $\delta\rho/\rho = 0.25$. We normalize the CDM spectrum so that the rms fluctuation in a sphere of radius 8 h^{-1} Mpc becomes equal to $\sigma_8 = 0.63$ at $z = 0$. The spheres are rigidly rotating and following the reduced Hubble expansion (see Steinmetz & Müller 1995). In these initial conditions, galaxies are formed in merging of small clumps, which is expected in the CDM universe, during the collapse of the initial spheres. However, there is no infall of gas and merging of subgalactic clumps after the collapse. These conditions can be valid for the formation of isolated field galaxies and galaxies formed in a low-density universe ($\Omega_0 < 1$). Two free parameters, mass and spin parameter, are listed in Table 2.

The gas and dark matter are represented by the same number of particles, and their mass ratio is set to $\frac{1}{9}$. The initial temperature of the gas is set to 70 K of the cosmic microwave background at $z = 25$. The mass of a gas particle varies between 2.4×10^6 and $1.9 \times 10^7\ M_\odot$ according to the system mass considered (Table 2). The mass of a dark matter particle varies between 2.1×10^7 and $1.7 \times 10^8\ M_\odot$. Low resolution may cause an artificial heating due to two-body relaxation between the SPH and dark matter particles, however this range of particle mass is small enough to exclude the artificial heating effect (Steinmetz & White 1997). The gravitational softenings are taken to be 1.5 kpc for gas and star particles, and 3 kpc for dark matter. The total number of particles typically becomes $\sim 4 \times 10^4$ at the end of the simulations ($z = 0$).

TABLE 1

ENERGY, MASS, AND METAL RELEASED PER STAR

Type	$E_{\rm rls}$ (ergs star^{-1})	$M_{\rm rls}$ ($M_\odot$ star^{-1})	$Mz_{\rm rls}$ ($M_\odot$ star^{-1})	Period (10^8 yr)
SW	10^{49}	...	...	0–0.4
SNIa...	10^{51}	1.4	1.4	0–0.4
SNII ...	10^{51}	15.3	2.5	5–30

NOTE.—A star with $\geq 8\ M_\odot$ is assumed to release the total energy $E_{\rm rls}$, mass $M_{\rm rls}$, and metal $Mz_{\rm rls}$ through stellar wind (SW), Type Ia (SNIa), and Type II (SNII) suparnovae. The values listed above are averaged over stars distributed according to the Salpeter's IMF, using the yield tables of nucleosynthesis (Nomoto et al. 1997a, 1997b). We set the upper (lower) mass cut of the IMF to 60 $M_\odot$ (0.1 $M_\odot$). The number of stars with $\geq 8\ M_\odot$ in a *star particle* can be estimated with the Salpeter's IMF.

TABLE 2

CATALOG OF SIMULATED GALAXIES

Run	M ($M_\odot$)	λ	$\delta\rho/\rho$	W_{20} (km s^{-1})	M_I (mag)
1.....	8×10^{11}	0.10	1.9 σ	466	−22.31
2.....		0.08	1.9 σ	524	−22.07
3.....		0.06	1.9 σ	549	−21.90
4.....	4×10^{11}	0.08	1.7 σ	420	−21.32
5.....		0.06	1.7 σ	437	−21.21
6.....		0.04	1.7 σ	454	−21.06
7.....	2×10^{11}	0.10	1.5 σ	299	−20.78
8.....		0.08	1.5 σ	331	−20.66
9.....		0.06	1.5 σ	342	−20.47
10.....		0.04	1.5 σ	349	−20.34
11.....	1×10^{11}	0.10	1.4 σ	236	−20.09
12.....		0.08	1.4 σ	248	−19.92
13.....		0.06	1.4 σ	257	−19.80
14.....		0.04	1.4 σ	254	−19.66

NOTE.—Our two initial free parameters, total mass M and spin parameter λ, initial overdensity $\delta\rho/\rho$ above the background field, and two observable values of final galaxies, line width W_{20} and I-band total magnitude M_I, are listed.

2.3. *Data Reduction*

In order to compare the properties of observed and simulated galaxies, we compute the observables such as luminosity and the line width for each "spiral galaxy" at $z = 0$. Stellar luminosity is computed with the simple stellar population (SSP) synthesis models of Kodama & Arimoto (1997). The models provide integrated spectra along stellar isochrones corresponding to appropriate age and metallicity. We take the Salpeter's IMF. Total magnitude M_I of simulated galaxies is computed to sum up star particles using appropriate SSP tables, which are selected in accordance with age and metallicity of the star particles. The line width W_{20} is derived similarly to the observable as constructing a line profile of gas weighted by mass, and measuring the width at 20% level of a peak flux. The catalog of all the simulated galaxies is presented in Table 2.

3. RESULTS

3.1. *Evolution and Structures of Individual Galaxies*

Figure 1 shows snapshots of star particles at four redshifts for the case of $M = 4 \times 10^{11}\ M_\odot$ and $\lambda = 0.06$. These view angles provide a face-on projection at $z = 0$. Two clumps at $z = 4$ are merging and form a bulgelike system between $z = 4$ and 3. After the bulge formation, the surrounding gas gradually cools and falls to form a gaseous disk, and then a stellar disk is gradually formed. The panel at $z = 2$ shows that a disklike structure surrounds the central bulge. Since the gas density of the inner disk is higher than that of the outer part, the star formation timescale is shorter in the inner part than in the outer part. The

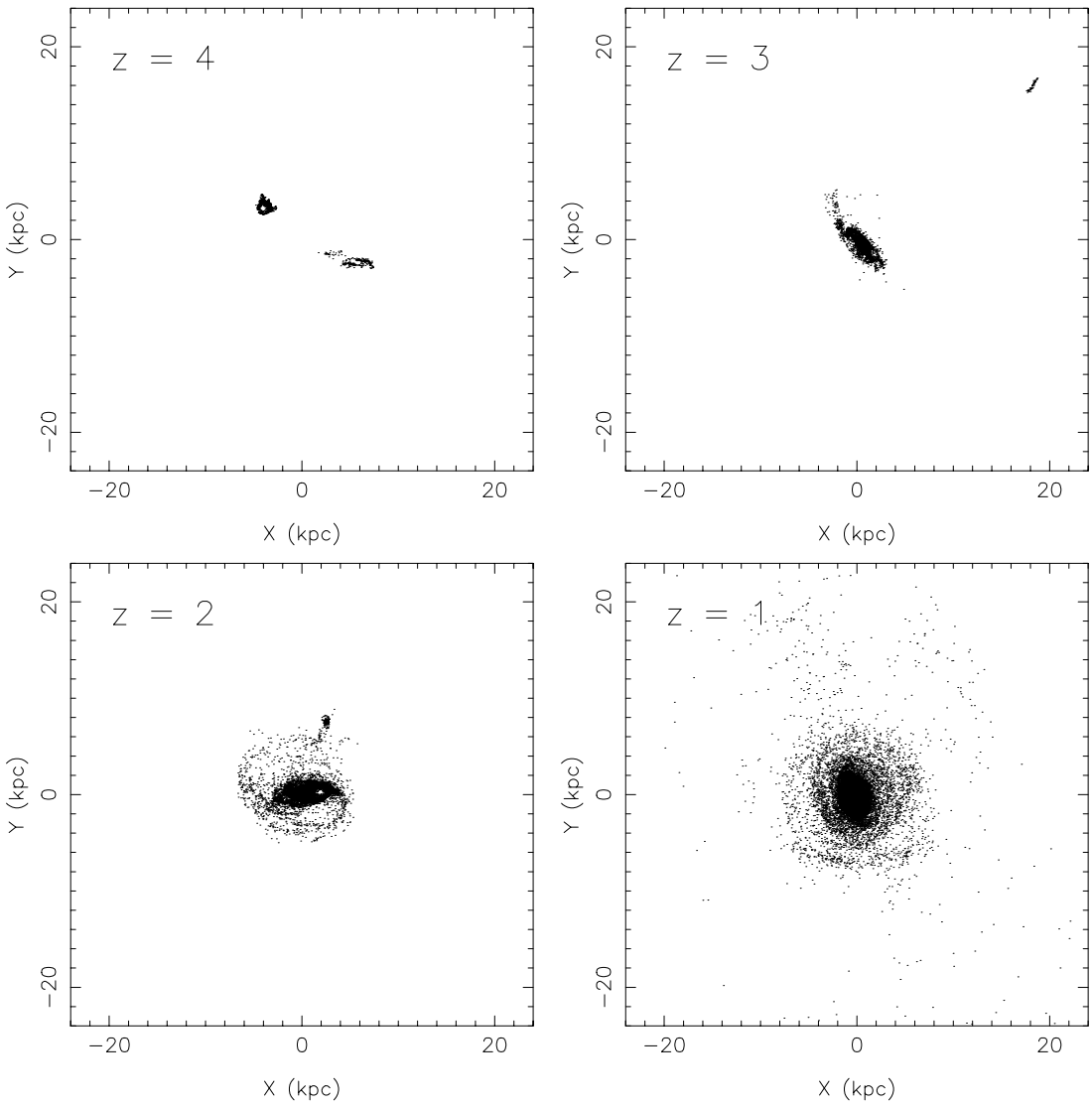

FIG. 1.—Snapshots of star particles at various redshifts in the case for $M = 4 \times 10^{11} M_{\odot}$ and $\lambda = 0.06$. The origin of each figure is shifted to make the object nearly at the center. The view angles give the face-on projection at $z = 0$. Note that these plots do not actually show the mass density because each star particle does not necessarily have the same mass.

stellar disk is gradually formed from the inside to outside in the gas disk. The panel at $z = 1$ shows a larger disk than that of $z = 2$.

In Figure 2 we plot the total star formation rate, total magnitude, and color in a rest frame against the look-back time (and also the redshift). The star formation rate peaks at $z \sim 3$ at a rate of 29 $M_{\odot}$ yr^{-1}, and then declines and reaches an almost constant value of 1 $M_{\odot}$ yr^{-1} at $z \sim 1$, when the stellar mass has already been about 80% of the total disk mass. At $z = 0$, about 10% of the total baryonic mass remains in the gas and the rest is already in stars, which is consistent with the observations of spiral galaxies. Total magnitude also peaks near the time of the maximum star formation. Then the magnitudes in all passbands are monotonically declining until $z = 0$, because the mean age of the stellar component becomes older and massive stars gradually die. The amount of the decline between $z = 3$ to the present is 1.6 mag in the I band.

We show the final snapshots of star particles in Figure 3. The I-band luminosity profile and rotation-velocity profile of the final galaxy are shown in Figure 4. Observed internal structures, such as the exponential light profile and flat rotation curve, are well reproduced as the results of the simulation. We confirm that all of the 14 simulated spiral galaxies attain such properties.

About 30% of total gas angular momentum transfers to that of dark matter in the period $z = 5$ to 2, when condensed gas core with dark halos merge into a larger object (Katz & Gunn 1991; Navarro, Frenk, & White 1995). After the period, the baryon disk scarcely loses the angular momentum, because of no infall of lumpy clumps in our simulations. The specific angular momenta of the baryon disks lie in the range of those in observed spiral galaxies at $z = 0$ (Fall 1983; Contardo et al. 1998). In the following discussion, we investigate a statistical property of 14 simulated galaxies, all of which have internal structures similar to observed spiral galaxies as discussed above.

3.2. *The Tully-Fisher Relation*

In Figure 5, we compare the observed (*open squares*) and simulated (*filled circles*) TF plot in the I band. We use the observed data presented by Han (1992) and translate

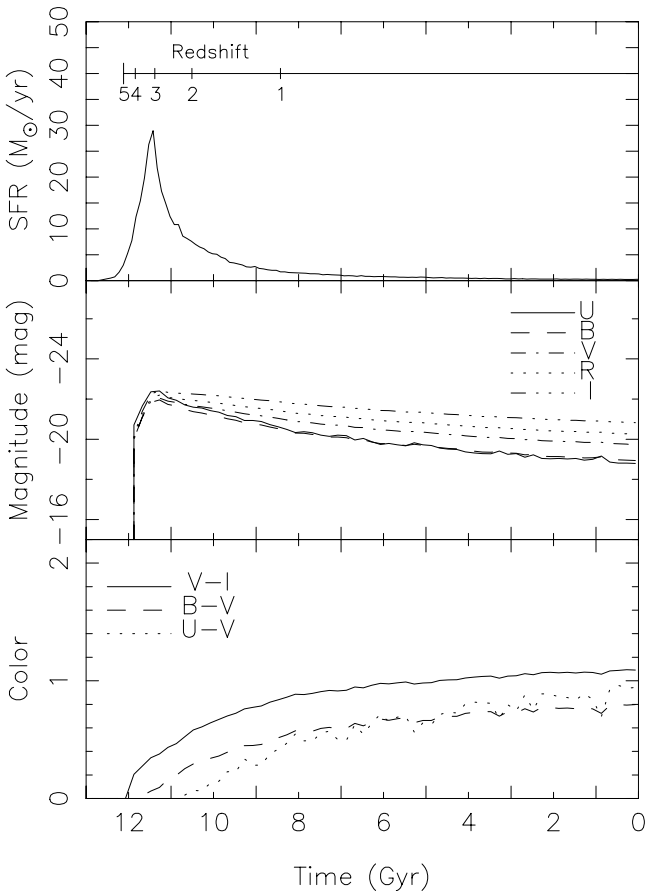

FIG. 2.—Evolution of total star formation rate, total magnitude, and color in the case for $M = 4 \times 10^{11}\ M_\odot$ and $\lambda = 0.06$. *Top*: Star formation rate vs. time. *Middle*: *U*-, *B*-, *V*-, *R*-, and *I*-band total magnitude in a rest frame vs. time. *Bottom*: $V-I$, $B-U$, and $U-V$ color in a rest frame vs. time. The scale in redshift is also illustrated in the top panel.

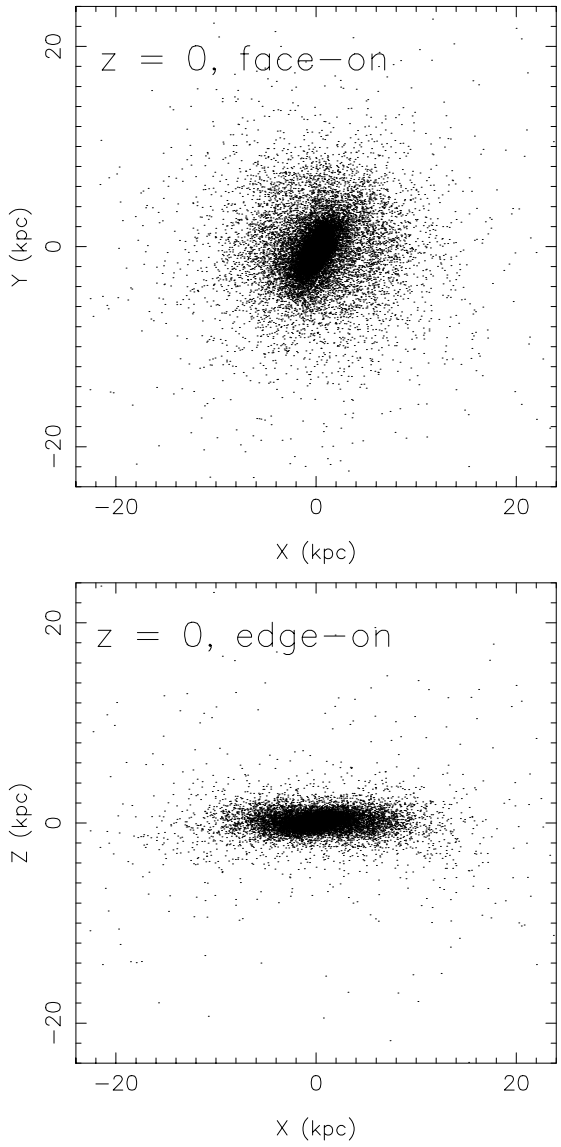

FIG. 3.—Snapshots at $z = 0$ of star particles in the case for $M = 4 \times 10^{11}\ M_\odot$ and $\lambda = 0.06$. *Top*: Face-on projection. *Bottom*: Edge-on projection. Note that this plot does not actually show the mass density because each star particle does not necessarily have the same mass.

them to absolute values with distances assuming $h = 0.5$. The slopes of the solid and dashed lines are derived by fitting to observed data (Giovanelli et al. 1997a), and the zero points are fitted by eye. In Figure 5, we notice that the simulated TF relation shows the following three points: (*a*) The slope of TF is well reproduced. (*b*) The scatter of TF is also similar to the observations. (*c*) The zero point is systematically fainter. These points are consistent with the previous results which included environmental effects, e.g., tidal field and infall/outflow of mass (Steinmetz & Navarro 1999). Here we artificially control initial conditions of isolated spheres, and examine how final structures of "spiral" galaxies depend on the initial conditions. Based on these simulations, we discuss the TF relation in detail on three points: the zero point, slope, and scatter.

1. The zero point: our simulated galaxies are 1.5 mag fainter than observed ones. We could find a possible solution of this discrepancy by changing the adopted cosmological model: changing h (Ω_0) would cause a vertical (horizontal) shift of the plotted points in Figure 5. If larger h (>0.5) is taken, distance estimations for the observed galaxies become smaller, and open squares (observed galaxies) vertically shift downward in Figure 5. If smaller Ω_0 (<1) is taken, the baryon fraction Ω_b/Ω_0 becomes larger because Ω_b should be fixed by big bang nucleosynthesis. Since *I*-band luminosity is almost determined by the total baryonic mass, it will result in a smaller mass-to-light ratio M/L, which shifts the filled circles (simulated galaxies) leftward in Figure 5. If we take a cosmological model with larger h (>0.5) and/or smaller Ω_0 (<1), which is suggested by recent observations (Giovanelli et al. 1997b; Perlmutter et al. 1998), the simulated TF relation would become consistent of the observed one. Note that the zero point also depends on the redshift when the whole mass is merging into a galaxy in hierarchical cosmology (Mo et al. 1998). The $\Omega_0 < 1$ universe will make this redshift later and shift the zero point brighter (upward). It also alleviates the discrepancy.

2. The slope: as seen in Figure 5, our simulations well reproduce the slope and scatter of the TF relation. The shifted zero point may not affect the mutual comparison among the simulated galaxies. In the left panel of Figure 6, the simulated galaxies with different masses are represented by different symbols on the TF plot. The slope of the solid

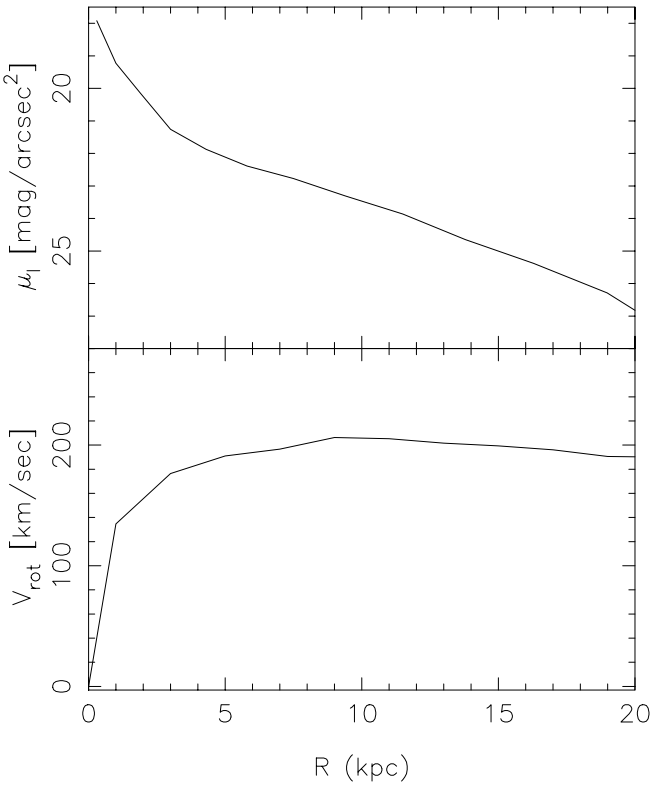

FIG. 4.—Internal structures of final galaxies at $z = 0$ in the case for $M = 4 \times 10^{11}\ M_\odot$ and $\lambda = 0.06$. *Top*: I-band surface brightness μ_I profile. *Bottom*: Rotation curve. All the simulated galaxies finally show the exponential light profiles and flat rotation curves, similar to observed spiral galaxies.

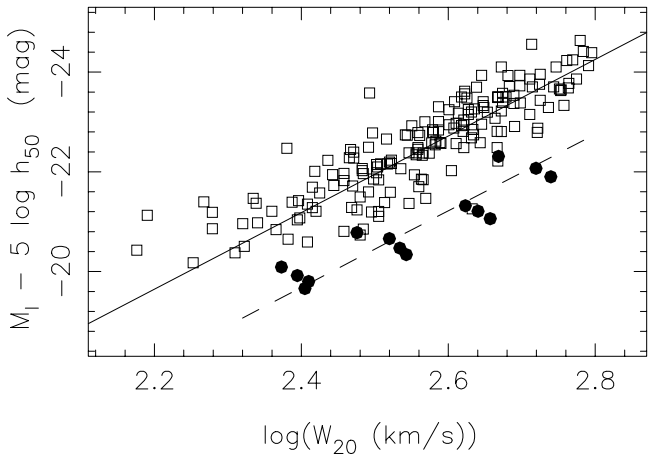

FIG. 5.—TF relation of the observed (*open squares*) and simulated galaxies (*filled circles*). The slopes of the solid and dashed lines are derived by fitting to observed data, and the zero points are fitted by eye. The observed galaxies can shift downward through the change of distance estimation if the present Hubble constant h_{50} in units of 50 km s^{-1} Mpc^{-1} is larger than 1. The simulated galaxies well reproduce the slope and scatter of the TF relation except for their 1.5 mag fainter zero point.

line is derived from observed data (Giovanelli et al. 1997a). Figure 6 clearly shows that larger total mass of galaxies result in brighter luminosity and larger line width. The resultant slope of model galaxies on the TF plot is quite similar to the observations. The TF correlation originates in the differences of total masses of galaxies.

3. The scatter: Figure 6 (*left*) shows that I-band luminosities are different among the galaxies with the same mass. The reason for the nonconstant M/L is found in the right panel of Figure 6. The right panel is the same plot as the left panel, but different symbols are used for different initial spin parameters λ. It shows that galaxies with different λ distribute nearly perpendicular to the TF correlation, resulting in the scatter of the TF relation. The amplitude of the scatter depends on the range of λ. We took $\lambda = 0.04$–0.10, which is a range if angular momenta are caused by the cosmological tidal field (Barnes & Efstathiou 1987). The role of spin parameters on the scatter can be explained in two ways: (*a*) Low (high) λ leads to a centrifugally concentrated disk, which provides large (small) line width W_{20}. (*b*) Low (high) λ results in smaller (larger) disk, and high (low) surface density of the gas disk, which controls the timescale of star formation τ_*. For low λ, τ_* is relatively short due to the high surface density, and most of stars are formed at the earlier phase of galaxy formation. Therefore, the mean age of the stellar component in low-λ galaxies is older than that in high-λ galaxies at $z = 0$. Low λ makes fainter galaxies

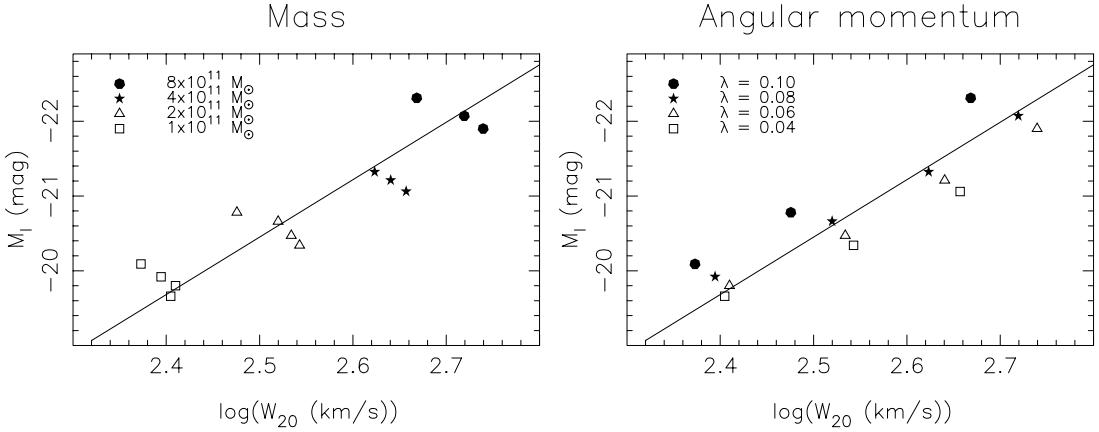

FIG. 6.—TF relations of simulated galaxies. The slopes of the solid lines are derived by fitting to observed data, and the zero point is fitted by eye. *Left*: Mass dependence of galaxy distribution in the TF plot. Different masses are explicitly shown with different symbols. The TF relation is extended to the direction that traces different masses. *Right*: Angular momentum dependence of galaxy distribution in the TF plot. Different spin parameters λ are shown with different symbols. Galaxies with different λ distribute nearly perpendicular to the TF relation and result in the scatter of the TF relation. The amplitude of the scatter depends on the range of λ. The range $\lambda = 0.04$–0.10, provided by the cosmological tidal field, results in the appropriate scatter.

than high λ through the age of their stellar component. This effect also makes the scatter of the TF relation.

4. SUMMARY AND DISCUSSION

We have investigated the origin of the TF relation by simulating formation of 14 galaxies with the N-body/SPH direct calculations, which includes the cooling, star formation, and stellar feedback. Internal structures of spiral galaxies, such as the exponential disk profile and flat rotation, are well reproduced as the results of the simulations, whereas these properties were assumed a priori in past semianalytic approaches (Mo et al. 1998; Heavens & Jimenez 1999). We *observed* the total magnitude and gas line widths of the simulated spiral galaxies, and found that they also reproduce the slope and scatter of the TF relation, except for the zero point. We have simulated galaxy formation from many different initial conditions, and found that the slope of the TF relation is produced by the difference of total galactic masses, and the scatter is produced by the difference of initial spin parameters.

We should comment upon our model of star formation and feedback. The following issues about star formation and feedback remain for future investigations with higher resolution simulations. Luminosity in red passbands is determined firstly by the stellar amount, and secondly by their age. Simulated galaxies have the stellar amount similar to the observations, typically $\sim 80\%$–90% of the total baryonic mass at $z = 0$. Hence, their luminosity depends on stellar-age distribution, i.e., star formation history. Our star formation model is based on Schmidt's law ($\dot{\rho}_* \propto \rho_{\rm gas}^{1.5}$), which is an optimal but robust model if the mean rate of star formation can be determined by a mean local density of the gas. This averaging treatment of star formation would be most suitable for the current resolution ~ 1 kpc. In the Milky Way, star formation is observed at molecular clouds, and further discussion about different kinds of star formation models would require to resolve at least the scale of molecular clouds $\lesssim 100$ pc, 10 times smaller than our spatial resolution. In our simulations, the star formation timescale is mostly set to $20\tau_{\rm dyn}$. Since the local dynamical timescale $\tau_{\rm dyn}$ is much shorter than galaxy age, the gas is transformed to stars efficiently in high redshift. Taking the model which gives longer timescales of star formation would provide brighter galaxies because galaxies that consist of younger stars are brighter.

Stellar feedback would control the self-regulation mechanisms in spiral galaxies as discussed by Silk (1997). Our adopted model behaved like a minimal feedback model, because of the feedback energy released as thermal energy that could be radiated away in a short timescale. If the energy is released as a kinetic form as discussed in Navarro & White (1993), the feedback would become more efficient and could change the history of star formation. However, it is not clear that feedback through kinetic energy occurrs in the scale of ~ 1 kpc, i.e., our spatial resolution. Since supernovae remnants expand to about 10–100 pc in the interstellar medium, 10–100 times higher spatial resolution than the present one should be required for the detailed modeling of the local stellar feedback. These issues remain for future investigations.

As discussed in § 3.2, the discrepancy of the 1.5 mag fainter zero point in the I band would be alleviated in the cosmological model of $h > 0.5$ and $\Omega_0 < 1$. We should note, however, that this discrepancy cannot be solved in the $h = 0.5$ and $\Omega_0 = 1$ cosmology with different models of star formation and feedback. The I-band luminosity declines by only 1.6 mag from $z = 3$, the time of the peak luminosity, to the present. In order to shift the zero point 1.5 mag brighter by changing the star formation history, almost all the stars must be formed at very low redshift $z < 0.1$ (recent 2 Gyr) in all the spiral galaxies in the local universe.

Our initial conditions represent the collapse of galaxy-scale isolated overdense regions. Under these idealized initial conditions, the merging of subgalactic clumps and tidal interaction between galaxies at $z \lesssim 2$, which is expected in the $\Omega = 1$ CDM universe, cannot occur. Since major mergers can destroy a thin disk of galaxies, they would not involve the formation of disk galaxies. In other words, the TF relation would not be affected by major mergers and strong galaxy-galaxy interactions. This is also supported by the fact that our derived TF relation is consistent with the previous simulations (Steinmetz & Navarro 1999), which included the environmental effects, e.g., tidal field and infall/outflow of mass. However, a continuous gas supply and minor mergers could affect the simulations, enhancing the star formation rate at a low redshift. They will make galaxies brighter, and alleviate the zero-point problem discussed in § 3.2. In our isolated initial conditions, the simulations do not suffer from an extreme transfer of angular momentum from baryon to dark matter (Navarro et al. 1995; Navarro & Steinmetz 1997) because no merging occurs at a low redshift. The transfer of angular momentum might be a problem if we consider the galaxy formation in a larger volume.

Numerical computations were carried out on the GRAPE-3 system at the Astronomical Data Analysis Center of the National Astronomical Observatory, Japan. J. K. thanks the Hayakawa Fund of the Astronomical Society of Japan for the financial support to participate the 15th IAP meeting. We would like to thank N. Arimoto for providing us with their tables of the stellar population synthesis. We thank M. Honma for reading the manuscript. We also thank the anonymous referee for giving helpful comments.

REFERENCES

Barnes, J., & Efstathiou, G. 1987, ApJ, 319, 575
Contardo, G., Steinmetz, M., & Fritze-von Alvensleben, U. 1998, ApJ, 507, 497
Fall, S. M. 1983, in IAU Symp. 100, Internal Kinematics and Dynamics of Galaxies, ed. E. Athanassoula (Dordrecht: Reidel), 391
Giovanelli, R., Haynes, M. P., da Costa, L. N., Freudling, W., Salzer, J. J., & Wegner, G. 1997b, ApJ, 477, L1
Giovanelli, R., Haynes, M. P., Herter, T., & Vogt, N. P. 1997a, AJ, 113, 53
Han, M. 1992, ApJS, 81, 35
Heavens, A. F., & Jimenez, R. 1999, preprint (astro-ph/9901016)
Katz, N. 1992, ApJ, 391, 502
Katz, N., & Gunn, J. 1991, ApJ, 377, 365
Katz, N., Weinberg, D. H., & Hernquist, L. 1996, ApJS, 105, 19
Koda, J., Wada, K., & Sofue, Y. 2000, in preparation
Kodama, T., & Arimoto, N. 1997, A&A, 320, 41
Mo, H. J., Mao, S., & White, S. D. M. 1998, MNRAS, 295, 319
Navarro, J. F., Frenk, C. S., & White, S. D. M. 1995, MNRAS, 275, 56
Navarro, J. F., & Steinmetz M. 1997, ApJ, 478, 13
Navarro, J. F., & White, S. D. M. 1993, MNRAS, 265, 271
Nomoto, K., et al. 1997a, Nucl. Phys. A, 616, 79c
———. 1997b, Nucl. Phys. A, 621, 467c
Perlmutter, S., et al. 1998, preprint (astro-ph/9812133)

Salpeter, E. F. 1955, ApJ, 121, 161
Silk, J. 1997, ApJ, 481, 703
Steinmetz, M. 1996, MNRAS, 278, 1005
Steinmetz, M., & Müller, E. 1994, A&A, 281, L97
———. 1995, MNRAS, 276, 549
Steinmetz, M., & Navarro, J. F. 1999, ApJ, 513, 555
Steinmetz, M., & White, S. D. M. 1997, MNRAS, 288, 545
Sugimoto, D., Chikada, Y., Makino, J., Ito, T., Ebiszaki, T., & Umemura, M. 1990, Nature, 345, 33
Tsujimoto, T., et al. 1995, MNRAS, 277, 945
Tully, R. B., & Fisher, J. R. 1977, A&A, 54, 661
Yoshii, Y., Tsujimoto, T., & Nomoto, K. 1996, ApJ, 462, 266
Zeldovich, Y. B. 1970, A&A, 5, 84